Characterization of opening angle correlations of a biphoton state decomposed in Bessel modes

Baghdasar Baghdasaryan [1,*], Fabian Steinlechner,[2,3] and Stephan Fritzsche[1,4]

[1]*Theoretisch-Physikalisches Institut, Friedrich-Schiller-Universität Jena, D-07743 Jena, Germany*
[2]*Fraunhofer Institute for Applied Optics and Precision Engineering IOF, Albert-Einstein-Strasse 7, 07745 Jena, Germany*
[3]*Abbe Center of Photonics, Friedrich-Schiller-University Jena, Albert-Einstein-Strasse 6, 07745 Jena, Germany*
[4]*Helmholtz-Institut Jena, D-07743 Jena, Germany*

The spontaneous parametric down-conversion of photons has been widely applied for generating entangled photon pairs. We theoretically explore the entangled down-converted state of the photon pair, also known as *biphoton* state, for both degenerate and nondegenerate photon pairs. In particular, the spatial structure of the biphoton state has been expressed in Bessel modes to better understand the correlation with regard to the opening angle ϑ_k of Bessel modes. In fact, the opening angles of the down-converted photon pair are not independent of each other, but rather are correlated. Furthermore, we confirm the experimentally observed conditions concerning the optimization of generating high-degree spatial entanglement by controlling the beam waist of the pump beam. We also introduce a new experimental setup for efficient measurement of the spatial entanglement of the biphoton state using geometrical optics arguments.

I. INTRODUCTION

Entanglement of quantum states is one of the most exciting features of quantum mechanics and has been widely exploited in many applications, such as quantum cryptography [1], quantum teleportation [2], or quantum computing [3]. Experimentally, for instance, spontaneous parametric down-conversion (SPDC) has been a reliable process for the generation of entangled photon pairs or nondiffracting *heralded* single photons [4]. Indeed, SPDC is a nonlinear optical process that converts the high-energy photons into entangled photon pairs by a nonlinear crystal and whose state is also called *biphoton* state. Moreover, SPDC facilitates the generation of high-dimensional entangled states that are an essential ingredient in quantum information applications, as these states enlarge the information encoded in a single quantum system [5], enhance robustness against eavesdropping [6], and are more efficient by the distillation of important resource states for quantum computations [7].

Photons with well-defined orbital angular momentum (OAM), so-called *twisted* light, are described by high-dimensional Hilbert spaces. In the SPDC process, entanglement between spatial modes carrying OAM has been demonstrated experimentally [8,9] and theoretically [10–13]. In the *paraxial approximation,* Bessel beams carry well-defined OAM [14] and are known to be more robust to losses in the transmission of entangled states at long distances. Moreover, the measured degree of entanglement in the Bessel modes recovers when an obstruction is encountered along the beam (self-healing) [15]. Self-healing of Bessel beams has also been used to demonstrate hybrid high-dimensional quantum key distribution through obstacles

with self-reconstructing single photons [16]. Therefore, the detailed investigation of the Bessel modes is of direct interest in quantum protocols. Here, we want to emphasize a property of Bessel modes that is important for this work.

Monochromatic Bessel beams do (formally) not diffract; that is, the values of the transversal and longitudinal components of the linear momentum are fixed along the beam. As a consequence, all wave vectors $\boldsymbol{k}$ of the Bessel beam lie on a cone with an opening angle of ϑ_k [17]. Therefore, the opening angle is characteristic for a single and monochromatic Bessel beam. In contrast to OAM, however, the opening angle is a continuous variable (CV). In general, the quantum states that consist of a CV, live in an infinite-dimensional Hilbert space and extend quantum communication protocols to infinite dimensions. Here, the primary motivation for dealing with continuous variables in quantum information concerns an efficient implementation of the essential steps in quantum communication protocols such as preparing, unitarily manipulating, and measuring entangled quantum states [18]. CV entanglement has been utilized by many experimental and theoretical studies [19–22]. We recommend for further reading the review article [23], where various ways of preparing CV quantum information, detecting CV quantum states, and operating onto the states have been introduced.

The Bessel modes have been used to represent the spatial correlations of photon pairs. In particular, the description of the radial degree of freedom by the transverse momentum of Bessel modes, which is a CV, has been a popular topic of investigations [24–26]. Here, we introduce a new approach, namely, the utilization of the opening angle of the Bessel beam to represent the radial degree of freedom. The opening angle and the radial momentum can be equivalently used for the description of Bessel modes. However, the main difference between the opening angle and the radial momentum is that the correlations regarding the opening angle depends on the
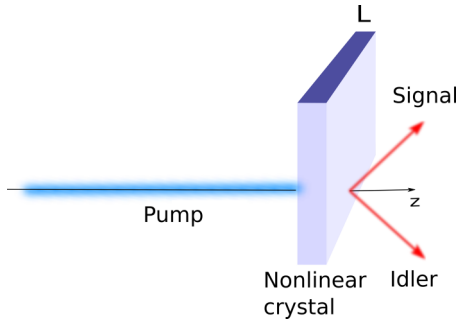
*baghdasar.baghdasaryan@uni-jena.de

FIG. 1. Setup of the SPDC process. A Gaussian beam of pump photons propagates along the z axis and interacts nonlinearly with a (nonlinear) crystal of length L to generate (down-converted) photons pairs. The red arrows represent the down-converted idler and signal photons whose state, also known as the biphoton state, is generally entangled.

ratio of energies of the down-converted photons in contrast to correlation regarding the radial momentum (Sec. II B). This fact can be useful for the direct investigation of nondegenerate SPDC process. We therefore express the spatial structure of the biphoton state in terms of Bessel modes. A possible normalization of Bessel modes has been introduced in Ref. [27] and the completeness and orthogonality have been introduced in Ref. [28].

As part of the work, we also analyze how the biphoton state depends on the shape of the pump beam, the length of the down-converting crystal, and the ratio of energies of photon pairs. From this, we obtain optimization conditions which can control the strength and the rate of correlation in opening angles of signal and idler photons. In Sec. III, moreover, we present an experimental setup that can be used to identify a particular θ_k by using an axicon lens. In the prior experimental work [25], the Bessel modes have been detected using spatial light modulators (SLMs). On the SLMs, encoded binary Bessel functions enable one to select a particular $\varkappa$ value with an efficiency of approximately 60%. However, the selection of θ_k is more informative as apart from the detection of a particular Bessel mode with high efficiency, one can also get information about the energy state of photons.

At the end of this section, we refer to several works in the field of spatial correlations to have a better overview of current research. Bessel modes are not the unique modes that have been used to describe the spatial correlations in SPDC. For instance, the transverse Hermite-Gauss [29–32], Laguerre-Gauss (LG) [33,34], or Ince-Gauss modes [35] have also been used to describe the spatial correlations in parametric down-conversion. We also refer to Ref. [36] for a compact overview of research in spatial correlations in SPDC.

II. THEORETICAL METHODS

A. The SPDC state

Figure 1 shows the setup of a typical SPDC process in which a second-order nonlinear crystal is illuminated by a quasimonochromatic laser pump beam (blue) and which propagates in the z direction. In the laboratory, the output of most lasers is a Gaussian beam, which can be described

by the fundamental zeroth-order transverse Gaussian mode. The down-converted lower-frequency photons (red) produced by SPDC are assumed to be monochromatic and fulfill the energy conservation $\omega_p = \omega_s + \omega_i$, which can be justified by choosing narrowband interference filters in front of the detectors. Here, the subscripts s and i indicate the two down-converted photons named *signal* and *idler*, while p refers to the pump photon.

In general, at the output of the nonlinear crystal, the biphoton state in the wave-vector domain can be expressed by [37]

$$|\Psi_{\mathrm{SPDC}}\rangle = \iint d\boldsymbol{k}_s \boldsymbol{k}_i \Phi(\boldsymbol{k}_s, \boldsymbol{k}_i) \hat{a}_s^\dagger(\boldsymbol{k}_s) \hat{a}_i^\dagger(\boldsymbol{k}_i) |00\rangle, \quad (1)$$

where the down-converted photons are described by the wave vectors $\boldsymbol{k}_s$ and $\boldsymbol{k}_i$, and where $\hat{a}_s^\dagger(\boldsymbol{k}_s)$ and $\hat{a}_i^\dagger(\boldsymbol{k}_i)$ are the creation operators for idler and signal photons, respectively, and $|00\rangle$ is the vacuum state. The function $\Phi(\boldsymbol{k}_s, \boldsymbol{k}_i)$, also called the phase-matching function, has the role of representing the coupling between the wave vectors, which results from the conservation of energy and momentum. These conversations are inherent in the parametric process, and therefore, the existence of the function $\Phi(\boldsymbol{k}_s, \boldsymbol{k}_i)$ is justified. How the function looks depends on the mode function of the pump beam and the properties of nonlinear crystal. The derivation of the phase-matching function has been discussed in detail [33,34,37]. Consequently, here, we should restrict ourselves to some basic formulas and notations required for the following discussion.

In the laboratory, the phase-matching condition $\delta \boldsymbol{k} = 0$ should be fulfilled in order to increase the efficiency of the generation of the SPDC in an optical setup. The momentum conservation in SPDC is given by

$$k_s + k_i = k_p = \frac{n_p \omega_p}{c} = \frac{n_s \omega_s}{c} + \frac{n_i \omega_i}{c}, \quad (2)$$

where n_p, n_s, and n_i are the refractive indices at the pump, signal, and idler wavelengths, respectively. In general, the condition (2) is difficult to fulfill with most materials as $n_s(\omega_s) < n_i(\omega_i) < n_p(\omega_p)$ for $\omega_s < \omega_i < \omega_p$. In order to overcome this issue, the setup of the experiment is usually realized with birefringent crystals, which may possess two or three different refractive indices for a given wavelength. Here, we consider the β-Ba(BO$_2$)$_2$ (BBO) uniaxial crystal with two crystal axes, which possess two different refractive indices, n_e (extraordinary) and n_o (ordinary). We consider the type-I phase matching, where idler and signal photons are both polarized in the ordinary direction and have the same polarization, while the pump photon is polarized in the extraordinary direction. In the following, we state some assumptions which allow us to determine the phase-matching function.

(i) The refractive indices at ordinary and extraordinary directions (the refractive indices at the pump, signal, and idler wavelengths) are equal: $n_{e,p} \approx n_{o,s} \approx n_{o,i}$. This is a good approximation for β-barium borate (BBO) crystal in the range of wavelengths $\lambda_p = 200$–1000 nm [38].

(ii) The transverse cross section of the nonlinear crystal is much larger than that of the pump beam. If this condition holds, the setup is invariant to translations in the plane of the crystal. Therefore, the phase-matching condition of the

transverse component of the wave vector $\boldsymbol{q}$ has to be satisfied, and the only phase mismatch is in the longitudinal direction.

(iii) The emitted angles between the z direction and the signal and idler beams are small enough to use the paraxial approximation by rewriting the z component of the momentum vector as $k_z = \sqrt{k^2 - |\boldsymbol{q}|^2} \approx k - |\boldsymbol{q}|^2/2k$.

With these all assumptions, the phase-matching function reads as [33]

$$\Phi(\boldsymbol{q}_s, \boldsymbol{q}_i) = \overbrace{\frac{w_p}{\sqrt{2\pi}} e^{-\frac{w_p^2}{4}|\boldsymbol{q}_s + \boldsymbol{q}_i|^2}}^{\text{Pump}}$$
$$\times \underbrace{\sqrt{\frac{2L}{\pi^2 k_p}} \operatorname{sinc}\left(\frac{L|\boldsymbol{q}_s - \boldsymbol{q}_i|^2}{4k_p}\right) e^{-i\frac{L}{4k_p}|\boldsymbol{q}_s - \boldsymbol{q}_i|^2}}_{\text{Phase Matching}}, \quad (3)$$

where L stands for the finite thickness of the crystal in the longitudinal direction and k_p stands for the wave vector of the pump beam.

Next, we should explore the spatial structure of the biphoton state, which is usually done by mode decomposition of the photons' joint wave function using a complete and orthogonal basis of transverse optical modes. The choice of such kind of basis is justified due to the paraxial nature of experiments.

The signal and idler photons are naturally entangled in arbitrary superposition's of OAM modes, which was shown theoretically [10,11] and experimentally [8]. Therefore, it is natural to choose for the decomposition of the biphoton state a basis that carries OAM. The theoretical Bessel modes, which carry OAM, have been used for discussion of various experiments. In particular, the simple mathematical description of these modes made them very attractive for theoretical calculations. Here, therefore, we explore the biphoton state given in Bessel modes, where our primary purpose is not only to show that the photon pairs are OAM correlated but also to expand this description by considering another characteristic number of Bessel modes as a possible correlated variable in the SPDC process, namely, the opening angle ϑ_k.

Bessel modes generally represent a nonparaxial solution of the Helmholtz equation. A photon in a Bessel mode can be described by

$$|\varkappa, \ell\rangle = \int d\boldsymbol{q} \, a_{\varkappa\ell}(\boldsymbol{q}) \hat{a}^\dagger(\boldsymbol{q}) |0\rangle,$$

where $a_{\varkappa l}(\boldsymbol{q})$ is the Bessel mode given in momentum space:

$$a_{\varkappa\ell}(\boldsymbol{q}) = \sqrt{\frac{2\pi}{\varkappa}} (-i)^\ell e^{i\ell\varphi_q} \delta(q - \varkappa). \quad (4)$$

These Fourier coefficients are indexed by the modulus of the transverse momentum $\varkappa = |\boldsymbol{q}|$ and the projection of the OAM, ℓ, onto the beam axis.

We explore the biphoton state when the signal and idler photons are given in Bessel modes characterized by the pairs $(\varkappa_s, \ell_s)$ and $(\varkappa_i, \ell_i)$, respectively. Thus, the coincidence amplitude can be written as

$$C_{\varkappa_s, \varkappa_i}^{\ell_s, \ell_i} = \iint \langle \ell_s, \varkappa_s; \ell_i, \varkappa_i | \Psi_{\text{SPDC}} \rangle$$
$$= \iint d^3\boldsymbol{q}_s d^3\boldsymbol{q}_i \Phi(\boldsymbol{q}_s, \boldsymbol{q}_i) [a_{\varkappa_s \ell_s}(\boldsymbol{q}_s)]^* [a_{\varkappa_i \ell_i}(\boldsymbol{q}_i)]^*. \quad (5)$$

Moreover, the coincidence probability for finding the signal and idler photons characterized by modes $(\varkappa_s, \ell_s)$ and $(\varkappa_i, \ell_i)$ is given by $P_{\varkappa_s, \varkappa_i}^{\ell_s, \ell_i} = |C_{\varkappa_s, \varkappa_i}^{\ell_s, \ell_i}|^2$.

For calculations, it is convenient to represent the integral (5) in cylindrical coordinates, hence we rewrite the transverse component $\boldsymbol{q}$ in the following way,

$$\boldsymbol{q}_{s,i} = \begin{pmatrix} \rho_{s,i} \cos\varphi_{s,i} \\ \rho_{s,i} \sin\varphi_{s,i} \\ 0 \end{pmatrix},$$

and find the following for the coincidence amplitude,

$$C_{\varkappa_s, \varkappa_i}^{\ell_s, \ell_i} \propto \int_0^\infty \int_0^\infty \int_0^{2\pi} \int_0^{2\pi} \Phi(\rho_s, \rho_i, \varphi_s, \varphi_i) [a_{\varkappa_s \ell_s}(\rho_s, \varphi_s)]^*$$
$$\times [a_{\varkappa_i \ell_i}(\rho_i, \varphi_i)]^* \rho_s \rho_i \, d\rho_s \, d\rho_i \, d\varphi_s \, d\varphi_i. \quad (6)$$

Next, we do the following substitution in the expression of the phase-matching function (3),

$$|\boldsymbol{q}_s \pm \boldsymbol{q}_i|^2 = \rho_s^2 + \rho_i^2 \pm 2\rho_s\rho_i \cos(\varphi_s - \varphi_i),$$

and rewrite it as

$$\Phi(\rho_s, \rho_i, \varphi_s, \varphi_i) = \frac{w_p}{\sqrt{2\pi}} e^{-\frac{w_p^2}{4}[\rho_s^2 + \rho_i^2 + 2\rho_s\rho_i \cos(\varphi_s - \varphi_i)]} \sqrt{\frac{2L}{\pi^2 k_p}}$$
$$\times \operatorname{sinc}\left(L\frac{\rho_s^2 + \rho_i^2 - 2\rho_s\rho_i \cos(\varphi_s - \varphi_i)}{4k_p}\right)$$
$$\times e^{-i\frac{L}{4k_p}[\rho_s^2 + \rho_i^2 - 2\rho_s\rho_i \cos(\varphi_s - \varphi_i)]}. \quad (7)$$

The function $\Phi(\rho_s, \rho_i, \varphi_s, \varphi_i)$ depends on ρ_s and ρ_i, and on the difference of the azimutal angles $\varphi_s - \varphi_i$. Hence, we can expand this function as the superposition of plane waves with the phase $\exp[i\ell(\varphi_s - \varphi_i)]$:

$$\Phi(\rho_s, \rho_i, \varphi_s - \varphi_i) = \sum_{\ell=-\infty}^{\infty} f_l(\rho_s, \rho_i) e^{i\ell(\varphi_s - \varphi_i)}. \quad (8)$$

We substitute the new expression for the phase-matching function from Eq. (8) into Eq. (6) and first analyze only the angular integral over the angles φ_s and φ_i:

$$\sum_{\ell=-\infty}^{\infty} f_\ell(\rho_s, \rho_i) \int_0^{2\pi} \int_0^{2\pi} e^{-i(\ell_s\varphi_s + \ell_i\varphi_i)}$$
$$\times e^{i\ell(\varphi_s - \varphi_i)} d\varphi_s d\varphi_i \propto \delta_{\ell, \ell_s} \delta_{\ell, -\ell_i}. \quad (9)$$

The δ functions in Eq. (9) suggest to us to replace in Eq. (6) ℓ_s with ℓ and ℓ_i with $-\ell$. This guarantees the OAM conservation in the SPDC process: the entangled photons are perfectly anti-correlated in ℓ. For further calculations, we use the expression (7) as the expression (9) has been only introduced, in order to show the OAM conservation.

Next, we rewrite the *sinc* function in terms of the step function in the following way:

$$\operatorname{sinc}\left(\frac{L|\boldsymbol{q}_s - \boldsymbol{q}_i|^2}{4k_p}\right) = \frac{1}{L} \int_{-L/2}^{L/2} dt \exp\left(-\frac{i|\boldsymbol{q}_s - \boldsymbol{q}_i|^2 t}{2k_p}\right).$$

The integration in Eq. (6) over ρ_s and ρ_i is because of the δ function in the expression of Bessel modes (4); very simply, one should replace ρ_s and ρ_i with $\varkappa_s$ and $\varkappa_i$, respectively.

Furthermore, we use the integral representation of the Bessel function of the first kind for the angular integration [39]:

$$J_n(z) = \frac{1}{2\pi} \int_0^{2\pi} e^{i(z\sin\varphi - n\varphi)} d\varphi.$$

Our final result for the degenerate biphoton state is given by

$$C^{\ell,-\ell}_{\varkappa_s,\varkappa_i} \propto \frac{w_p}{\sqrt{L}} \sqrt{\varkappa_s \varkappa_i} \int_{-L/2}^{L/2} dt J_\ell[\varkappa_s \varkappa_i A(t)] e^{B(t)(\varkappa_s^2 + \varkappa_i^2)}, \quad (10)$$

where

$$A(t) = -iw_p^2/2 - L/(2k_p) - t/k_p,$$

$$B(t) = -w_p^2/4 - iL/(4k_p) - it/(2k_p).$$

In order to obtain the coincidence amplitude for the nondegenerate biphoton state, one should replace the expression $|\boldsymbol{q}_s - \boldsymbol{q}_i|^2$ in the last two terms of Eq. (3) by $|\boldsymbol{q}_s\omega_i/\omega_s - \boldsymbol{q}_i\omega_s/\omega_i|^2$ and perform the analog steps described before (see the Appendix).

For further discussion, we consider instead the opening angle of the Bessel mode, which is fully defined by $\varkappa$ for the given energy ω:

$$\vartheta_k(\varkappa) = \arctan\left[\frac{\varkappa}{\sqrt{\omega^2/c^2 - \varkappa^2}}\right]. \quad (11)$$

In SPDC, the *real* correlated parameter is the radial momentum. However, we *translate* the correlation regarding the radial momentum into the correlation in the opening angle using Eq. (11). The goal is to use the dependence of the opening angle on the energy of photons, in order to investigate the nondegenerate SPDC process. In Sec. III, an experimental setup for the detection of the opening-angle correlation is introduced, in order to make our discussion complete. In the following, we explore the correlation between $\vartheta_{k,s}$ and $\vartheta_{k,i}$ by analyzing the coincidence amplitude from Eq. (10). The integral in Eq. (10) is evaluated numerically. However, by considering the thin crystal approximation, one can find an analytical expression for the coincidence amplitude using the fact that the integration limits depend on the crystal length L.

B. Results and discussion

Expression (10) represents the spatial structure of the biphoton state if expressed as a superposition of Bessel modes. In detail, we consider the correlation in the opening angle of Bessel beams, which depends on parameters such as the OAM of signal and idler photons, the pump beam waist, the crystal length, and the ratio of the energies of the signal and idler photons. We choose for the wavelength of the pump beam $\lambda_p = 413$ nm, which is a typical value in experiments.

Let us start the discussion from the comparison of our results with similar calculations, where the spatial structure of the biphoton state was described in Laguerre-Gauss modes. Figure 3 displays the coincidence probability $P^{\ell_s,\ell_i}_{\vartheta_{k,s},\vartheta_{k,i}}$ of Bessel modes (upper panels) discussed in the previous section and $P^{\ell_s,\ell_i}_{p_s,p_i}$ of LG modes (lower panels) derived in Ref. [33]. The highest probabilities of selecting a joint state of a given OAM, $|\ell|$, are located along the diagonals of the graphs, where
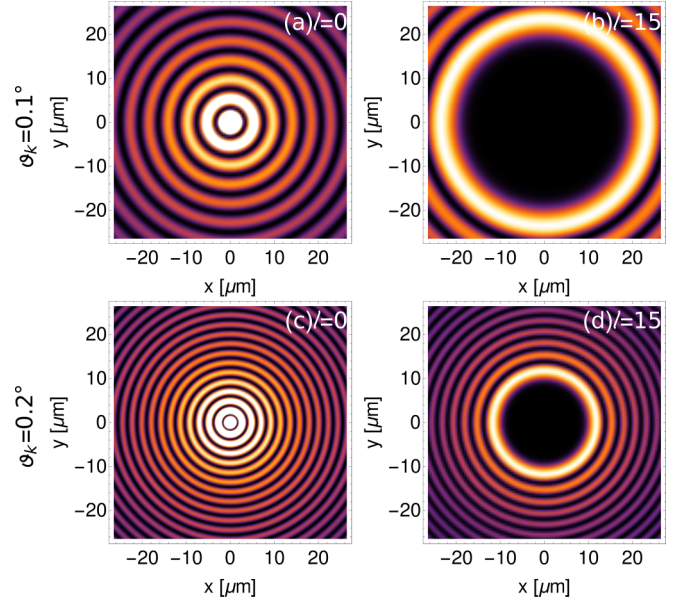

FIG. 2. Intensity profiles of Bessel beams in the *x*-*y* plane at $z = 0$. The radius and the amount of the rings in the certain area depend on the opening angle and the OAM of the Bessel beam. The graphs are shown for (a) the opening angle $\vartheta_k = 0.1°$ and the OAM $|\ell| = 0$, (b) for $\vartheta_k = 0.1°$ and $\ell = 15$, (c) for $\vartheta_k = 0.2°$ and $|\ell| = 0$, and (d) for $\vartheta_k = 0.2°$ and $|\ell| = 15$.

the values of the opening angles $\vartheta_{k,s}$ and $\vartheta_{k,i}$ or the radial indices p_s and p_i are equal. However, there is an optimal pair of opening angles or radial indices of given $|\ell|$ that maximize the coincidence probability. We also observe that the increase in the OAM causes a shift of the maximum probability to the higher values of ϑ_k and p. To understand this behavior, we should analyze Eq. (5) and Fig. 2. Here, we restrict ourselves to the discussion of Bessel modes because the arguments for the LG modes are analogous.

From Eq. (5) the coincidence amplitude depends on the product of the pump, idler, and signal modes, and our task is to understand the dependence of this product on the shape of these modes. By increasing the opening angle of the Bessel beam, the inner rings move toward the origin of the coordinates, where the Gaussian mode has the maximum value. Therefore, one could expect to have the maximum of the product of three modes in the region close to the origin. However, by increasing the opening angle, the width of the first ring, which has the maximum intensity, decreases, whereas the number of rings in a particular area increases. Consequently, there is an optimal pair of opening angles that maximize the product. Let us assume that the maximum is reached for a particular opening angle pair. Now, if one increases the value of the OAM, the radius of the first ring would increase (see Fig. 2) and move away from the origin. Therefore, in order to maximize the product again, the rings have to move toward the origin of the coordinates, which can be done by increasing the opening angle. To summarize, the maximum of coincidence probability moves to higher values of ϑ_k when the OAM of the SPDC pair increases. All arguments are also right for LG modes characterized by the radial index. We conclude that the change in the OAM affects
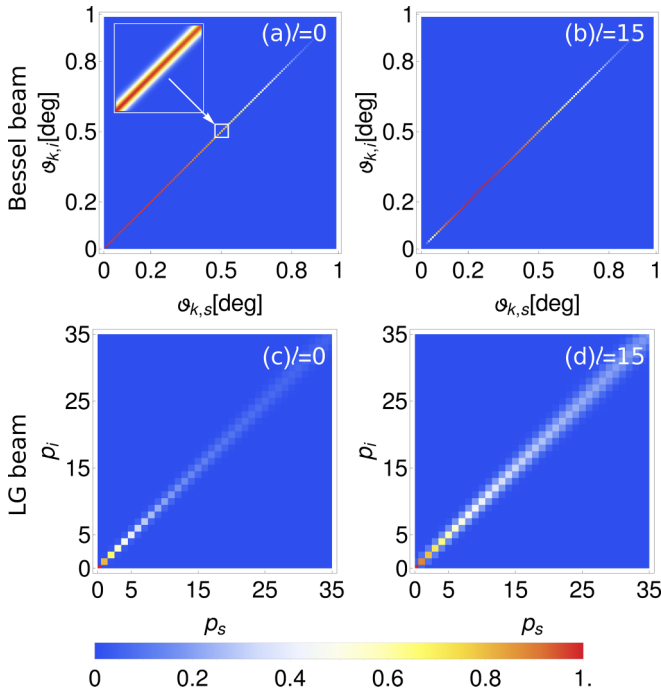
FIG. 3. Correlation between $\vartheta_{k,s}$ and $\vartheta_{k,i}$ (upper panel) and between p_s and p_i derived in Ref. [33] (lower panel) for different values of the OAM $|\ell|$ and the degenerate photon pair. The chosen values for the pump beam waist and the crystal length are $w_p = 3200$ μm and $L = 2$ mm, respectively. The highest probability is expected along the diagonal for both parameters, which shifts along the diagonal as long as the absolute value of the OAM $|\ell|$ increases. In contrast to the radial index p, the opening angle is a continuous variable, which is shown enlarged on the first graph. The high value of the OAM, $|\ell| = 15$, is chosen for a better demonstration of the shifting of maxima. The normalization is done for each graph individually. The normalization in Figs. 4, 5, and 6 is done in the same way.

similar changes in intensity profiles and also in coincidence probabilities displayed in Fig. 3. In that sense, the opening angle of Bessel modes and the radial index of LG modes are analogous parameters. One could expect this, keeping in the mind that both θ_k and p represent the radial degree of freedom of a photon. However, a massive difference exists between the correlations in the opening angle of Bessel modes and the radial index of LG modes: in contrast to the radial index of
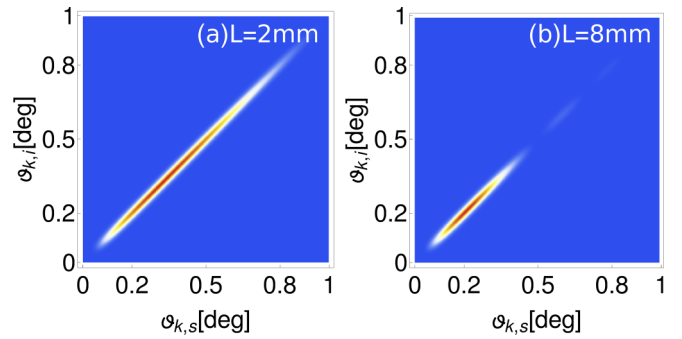

FIG. 5. The same as in Fig. 4 but for different crystal lengths: $L = 2$ and 8 mm. The calculations have been performed for the pump beam waist $w_p = 320$ μm and the OAM $|\ell| = 4$. By increasing the crystal length, the correlation between opening angles of signal and idler beams vanishes along the diagonal for large opening angles.

LG modes, the opening angle of Bessel modes describes a continuous variable, which can be beneficial in the quantum protocols because of the arguments mentioned in Sec. I.

Next, we discuss the influence of the pump beam waist on the coincidence probability. From Fig. 4 it follows that the increase in w_p yields to δ correlation between $\vartheta_{k,s}$ and $\vartheta_{k,i}$. Moreover, an idealized plane-wave pump in the process of SPDC would lead to strict correlations so that each signal mode would correspond to a single idler mode. However, the crystal size places an effective upper limit on the beam waist and makes impossible the use of an arbitrary large waist.

A second-order nonlinear process, such as SPDC, depends on the intensity of incident light. If the intensity is sufficiently low, then no nonlinearity is observed in the experiment. By decreasing the pump beam waist, one increases the intensity of the incident light and gives rise to second-order nonlinearity. With this in mind, we notice from Fig. 4 that the probability for photon pairs to have different opening angles increases, which means the number of photons coupled into a single-mode system increases. Our results agree with previous experimental work introduced in Ref. [26].

Furthermore, we discuss the dependence of the biphoton state on the crystal length. The correlation probability along the diagonal of the graph from Fig. 5 vanishes for large opening angles when the length of the crystal increases. A reason for this behavior could be the path length of photons
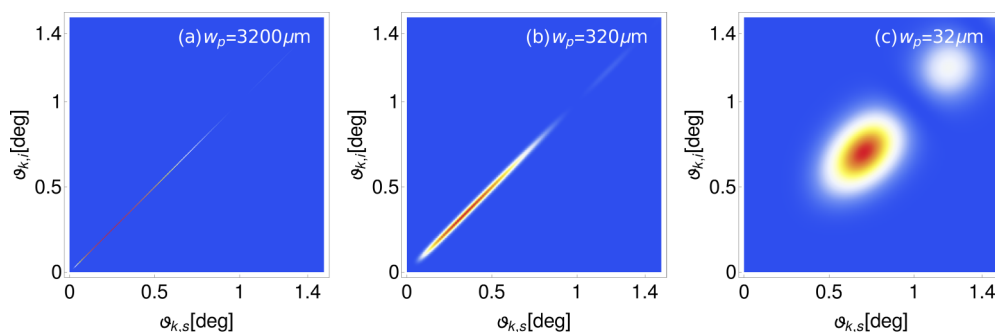

FIG. 4. The same as Fig. 3 but for Bessel modes with the OAM $\ell = 4$ and different beam waits of the pump beam: $w_p = 32$, 320, and 3200 μm. These graphs show that better focusing of the pump beam increases the amount of *nondiagonal* correlated pairs. If the beam waist increases, the strength of the correlation also increases and for infinitely large beam waist (plane wave) leads to δ correlation.
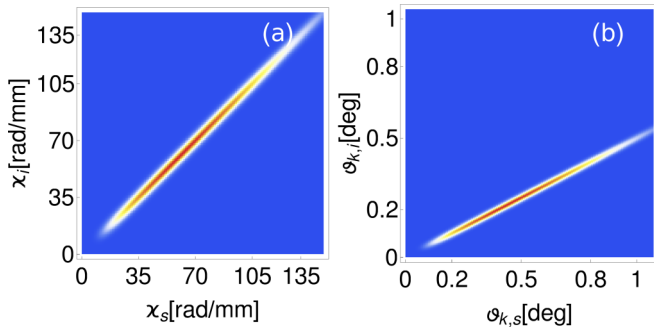
FIG. 6. The same as in Fig. 4 but for the correlation (a) between the modulus of transverse momentum of signal and idler photons, $\varkappa_s$ and $\varkappa_i$, and (b) between $\vartheta_{k,s}$ and $\vartheta_{k,i}$ for nondegenerate photon pairs with energies $\omega_i = 2\omega_s = 2\omega_p/3$. The correlation regarding the opening angle in contrast to the transverse momentum correlation depends strongly on the ratio of the photon pair energies w_i/w_s.
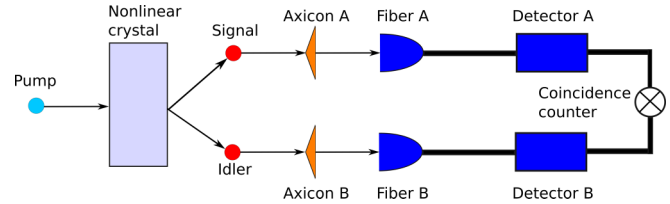

FIG. 7. Experimental setup for the detection of a zeroth-order Bessel mode. After parametric down-conversion, each of the photons enters a mode detector consisting of an axicon and a monomode optical fiber. By diffraction at the axicon, the incoming mode undergoes a mode transformation in such a way that a Bessel mode can be transformed into a Gaussian mode. Only the Gaussian mode can be coupled into the monomode fiber, as all Bessel modes have a larger spatial extension. The measurements should be performed in coincidence detection between the two down-converted photons.

in the crystal. For small opening angles, the probability is high that the photon would take a shorter path in the crystal. Moreover, the path length in the crystal enhances faster for the large opening angles with the length of the crystal, which means the influence of crystal properties can become stronger and lead to undesired nonlinearity. Second, from the experiments it is known that the efficiency of SPDC depends on the phase-matching condition, and there is an upper limit for wave-vector mismatch: $\delta\boldsymbol{k} = \boldsymbol{k}_p - \boldsymbol{k}_s - \boldsymbol{k}_i$. On the other hand, it is also known that the mismatch δk is antiproportional to the length of the interacting material, $|\delta\boldsymbol{k}| \propto 1/L$, which means that if one increases the length L, the upper limit conditions for $\delta\boldsymbol{k}$ becomes more strict. If the phase mismatch condition becomes more strict, fewer photons fulfill it, and the rate of SPDC decreases. We also recognize from Fig. 4 that better focusing of the pump beam causes similar changes on the correlation rate, namely, it leads to vanishing of correlation on the diagonal. This agrees with previous works, where it has been shown that the better focusing of the pump beam and the increasing of the crystal length implies similar changes in the correlation rate of the biphoton state [40,41].

Finally, we discuss the nondegenerate biphoton state. We considered idler and signal photons with the following energies: $\omega_s = \omega_p/3$ and $\omega_i = 2\omega_p/3$. The calculations showed that in contrast to the modulus of the transverse momentum $\varkappa$, the correlation regarding the opening angle depends strongly on the ratio of signal and idler photons energies (see Fig. 6). One should be careful in choosing the ratio of energies, in order to remain the condition $n_{e,p} \approx n_{o,s} \approx n_{o,i}$ as valid. We conclude that the measurement of the correlation as a function of the opening angle enables the analysis of the nondegenerated biphoton state. However, our calculations also show that the appearance of the degenerate biphoton state is the most probable scenario.

III. AN EXPERIMENTAL SETUP FOR DETECTING THE OPENING ANGLE CORRELATION

The use of the optical element axicon is a technique to generate an approximation to a zeroth-order Bessel beam with

efficiency close to 99% [42,43]. If a Gaussian beam illuminates the axicon with the beam size smaller than the hard aperture of the axicon, the whole input intensity is converted into an approximation to a Bessel beam. Higher-order Bessel beams also can be produced using LG beams to illuminate the axicon [44]. Axicons are characterized by the opening angle γ, which defines the opening angle of the Bessel beam produced by an axicon. The relation of these two angles is given by [45]

$$\theta_k = (n-1)\gamma, \tag{12}$$

where n is the refractive index of the axicon. Recently, a method was introduced to measure the small opening angles of axicons with high accuracy [46], which also ensures the well detection of the opening angle of a Bessel beam produced with an axicon. The simple relation (12) between the two opening angles motivates us to present an alternative experimental setup for the detection of Bessel modes, which is briefly presented in the following.

We use the fact that the transformation of light by axicons is ruled by geometrical optics arguments; that is, the Bessel beam can be used to produce a Gaussian beam if it propagates in the opposite direction through the axicon. The scheme of the setup is shown in Fig. 7. The mode detection of the down-converted photons should be performed for Bessel and Gaussian modes. The zeroth-order Bessel modes can be detected using an axicon with a defined opening angle and the Gaussian mode can be detected using monomode fibers in connection with avalanche detectors. Only the Gaussian modes can be coupled to the monomode fiber because all other spatial modes have a larger spatial extension. The detection and analysis of photon pairs can be measured with a coincidence counter.

A similar setup has been used in a prior work [25], where in SLMs encoded binary Bessel functions have been used to select a particular Bessel mode. However, using axicons remains the most efficient technique to generate Bessel modes. Moreover, the detection of Bessel modes by an axicon also gives information about the energy state of the photon.

IV. CONCLUSION

In this work, we investigated the biphoton state when its spatial structure was described in Bessel modes. In the previous works, the radial degree of freedom was described by the transverse momentum, which was here replaced by the opening angle of Bessel modes, in order to consider the nondegenerate SPDC process and detect radial correlations with a simple experimental scheme. The correlation in opening angles depends on the structure of the pump beam and also on the crystal properties. In particular, the good beam focusing or the long crystals reduce the rate of possible correlated pairs with the same values of opening angles. The pump beam waist also affects the strength of correlation and even leads to δ correlation between opening angles of the down-converted photons when the beam waist attends to infinity. Furthermore, we showed that this correlation strongly depends on the ratio of the energies of down-converted photons. Our investigations open up ways for high-dimensional entanglement experiments using continuous variables. An interesting future work concerns the extension of our work by replacing the Gaussian pump beam with the pump beam carrying OAM.

APPENDIX

Here, we briefly show how the ratio of energies of down-converted photon pairs comes into play if one considers the nondegenerate photon pairs. In a more general way, the phase-matching function is given by [33]

$$\Phi(\boldsymbol{q}_s, \boldsymbol{q}_i) = E(q_s + q_i)\sqrt{\frac{2L}{\pi^2 k_p}} \, \text{sinc}\left(\frac{L\Delta k_z}{2}\right)e^{-i\frac{L\Delta k_z}{2}},$$

where $E(q_s + q_i)$ is the Fourier transform of the spatial distribution of the pump at the input face of the crystal. Now using the paraxial approximation $k_z = \sqrt{k^2 - |\boldsymbol{q}|^2} \approx k - |\boldsymbol{q}|^2/2k$, Eq. (2), and the assumption $n_{e,p} \approx n_{o,s} \approx n_{o,i}$, one can replace Δk_z with

$$\Delta k_z \approx \frac{|\boldsymbol{q}_s \omega_i/\omega_s - \boldsymbol{q}_i \omega_s/\omega_i|^2}{2k_p},$$

which was done in Eq. (3) for $\omega_s = \omega_i$.

[1] R. Ursin, F. Tiefenbacher, T. Schmitt-Manderbach, H. Weier, T. Scheidl, M. Lindenthal, B. Blauensteiner, T. Jennewein, J. Perdigues, P. Trojek, B. Ömer, M. Fürst, M. Meyenburg, J. Rarity, Z. Sodnik, C. Barbieri, H. Weinfurter, and A. Zeilinger, Nat. Phys. **3**, 481 (2007).

[2] D. Bouwmeester, J.-W. Pan, K. Mattle, M. Eibl, H. Weinfurter, and A. Zeilinger, Nature (London) **390**, 575 (1997).

[3] M. A. Nielsen and I. L. Chuang, *Quantum Computation and Quantum Information* (Cambridge University, Cambridge, England, 2000).

[4] H. Cruz-Ramírez, R. Ramírez-Alarcón, F. J. Morelos, P. A. Quinto-Su, J. C. Gutiérrez-Vega, and A. B. U'Ren, Opt. Express **20**, 29761 (2012).

[5] M. Erhard, R. Fickler, M. Krenn, and A. Zeilinger, Light: Sci. Appl. **7**, 17146 (2018).

[6] D. Kaszlikowski, P. Gnaciński, M. Żukowski, W. Miklaszewski, and A. Zeilinger, Phys. Rev. Lett. **85**, 4418 (2000).

[7] E. T. Campbell, H. Anwar, and D. E. Browne, Phys. Rev. X **2**, 041021 (2012).

[8] A. Mair, A. Vaziri, G. Weihs, and A. Zeilinger, Nature (London) **412**, 313 (2001).

[9] S. P. Walborn, A. N. de Oliveira, R. S. Thebaldi, and C. H. Monken, Phys. Rev. A **69**, 023811 (2004).

[10] H. H. Arnaut and G. A. Barbosa, Phys. Rev. Lett. **85**, 286 (2000).

[11] S. Franke-Arnold, S. M. Barnett, M. J. Padgett, and L. Allen, Phys. Rev. A **65**, 033823 (2002).

[12] C. K. Law and J. H. Eberly, Phys. Rev. Lett. **92**, 127903 (2004).

[13] X.-F. Ren, G.-P. Guo, B. Yu, J. Li, and G.-C. Guo, J. Opt. B: Quantum Semiclassical Opt. **6**, 243 (2004).

[14] B. Baghdasaryan, B. Böning, W. Paufler, and S. Fritzsche, Phys. Rev. A **99**, 023403 (2019).

[15] M. McLaren, T. Mhlanga, M. J. Padgett, F. S. Roux, and A. Forbes, Nat. Commun. **5**, 3248 (2014).

[16] I. Nape, E. Otte, A. Vallés, C. Rosales-Guzmán, F. Cardano, C. Denz, and A. Forbes, Opt. Express **26**, 26946 (2018).

[17] O. Matula, A. G. Hayrapetyan, V. G. Serbo, A. Surzhykov, and S. Fritzsche, J. Phys. B: At., Mol. Opt. Phys. **46**, 205002 (2013).

[18] S. Braunstein and P. Loock, Rev. Mod. Phys. **77**, 513 (2004).

[19] N. Korolkova, G. Leuchs, R. Loudon, T. C. Ralph, and C. Silberhorn, Phys. Rev. A **65**, 052306 (2002).

[20] M. Lassen, G. Leuchs, and U. L. Andersen, Phys. Rev. Lett. **102**, 163602 (2009).

[21] B. Coutinho dos Santos, K. Dechoum, and A. Z. Khoury, Phys. Rev. Lett. **103**, 230503 (2009).

[22] A. Pecoraro, F. Cardano, L. Marrucci, and A. Porzio, Phys. Rev. A **100**, 012321 (2019).

[23] U. L. Andersen, G. Leuchs, and C. Silberhorn, Laser Photonics Rev. **4**, 337 (2010).

[24] M. McLaren, J. Romero, M. J. Padgett, F. S. Roux, and A. Forbes, Phys. Rev. A **88**, 033818 (2013).

[25] M. McLaren, M. Agnew, J. Leach, F. S. Roux, M. J. Padgett, R. W. Boyd, and A. Forbes, Opt. Express **20**, 23589 (2012).

[26] W. P. Grice, R. S. Bennink, D. S. Goodman, and A. T. Ryan, Phys. Rev. A **83**, 023810 (2011).

[27] U. Jentschura and V. Serbo, Eur. Phys. J. C **71** (2011).

[28] Z. Yang, X. Zhang, C. Bai, and M. Wang, J. Opt. Soc. Am. A **35**, 452 (2018).

[29] S. P. Walborn, S. Pádua, and C. H. Monken, Phys. Rev. A **71**, 053812 (2005).

[30] X.-F. Ren, G.-P. Guo, J. Li, and G.-C. Guo, Phys. Lett. A **341**, 81 (2005).

[31] S. S. Straupe, D. P. Ivanov, A. A. Kalinkin, I. B. Bobrov, and S. P. Kulik, Phys. Rev. A **83**, 060302(R) (2011).

[32] S. Walborn and A. Pimentel, J. Phys. B: At., Mol. Opt. Phys. **45**, 165502 (2012).

[33] F. M. Miatto, A. M. Yao, and S. M. Barnett, Phys. Rev. A **83**, 033816 (2011).

[34] J. P. Torres, A. Alexandrescu, and L. Torner, Phys. Rev. A **68**, 050301(R) (2003).

[35] M. Krenn, R. Fickler, M. Huber, R. Lapkiewicz, W. Plick, S. Ramelow, and A. Zeilinger, Phys. Rev. A **87**, 012326 (2013).

[36] S. Walborn, C. Monken, S. Pádua, and P. S. Ribeiro, Phys. Rep. **495**, 87 (2010).

[37] B. E. A. Saleh, A. F. Abouraddy, A. V. Sergienko, and M. C. Teich, Phys. Rev. A **62**, 043816 (2000).

[38] D. N. Nikogosyan, Appl. Phys. A **52**, 359 (1991).

[39] H. A. Yousif and R. Melka, Comput. Phys. Commun. **106**, 199 (1997).

[40] R. Ramírez-Alarcón, H. Cruz-Ramírez, and A. B. U'Ren, Laser Phys. **23**, 055204 (2013).

[41] S. P. Walborn and C. H. Monken, Phys. Rev. A **76**, 062305 (2007).

[42] R. M. Herman and T. A. Wiggins, J. Opt. Soc. Am. A **8**, 932 (1991).

[43] V. Arrizón, U. Ruiz, D. Aguirre-Olivas, D. S. de-la Llave, and A. S. Ostrovsky, J. Opt. Soc. Am. A **31**, 487 (2014).

[44] Q. Sun, K. Zhou, G. Fang, Z. Liu, and S. Liu, Appl. Phys. B **104**, 215 (2011).

[45] D. McGloin and K. Dholakia, Contemp. Phys. **46**, 15 (2005).

[46] Y. Zheng, L. Chen, W. Fan, X. Hu, Z. Chen, and J. Pu, Appl. Sci. **9**, 3959 (2019).